SUGISAKA MASANORI

Journal of Robotics, Networking and Artificial Life
Vol. 11(1); May (2025), pp. 61–68
ISSN (Online): 2352-6386; ISSN (Print): 2405-9021
https://alife-robotics.org/jrnal.html

Research Article

# Parallel Finite Element Subdivision Method for Electromagnetic Analysis of a Large Interior Space

Nanako Mizoguchi[1], Kento Ohnaka[1], Hironobu Sugiyama[2], Shouichi Fujimoto[2], Sota Goto[3], Toshio Murayama[3], Amane Takei[1]

[1]*Graduate School of Engineering, University of Miyazaki, 1-1 Gakuen Kibanadai-Nishi, Miyazaki, Japan*
[2]*Faculty of Medicine, University of Miyazaki, 5200 Kihara, Kiyotake, Miyazaki, Japan*
[3]*Faculty of Engineering, University of Tokyo, 1-1 Gakuen Kibanadai-Nishi, Miyazaki, Japan*

ARTICLE INFO

*Article History*

Received 25 November 2022
Accepted 23 February 2025

*Keywords*

Parallel finite element method
Large-scale analysis
Full-wave electromagnetic field analysis
Mesh subdivision

ABSTRACT

In high-frequency electromagnetic field analysis, it is necessary to divide the waveform into elements whose maximum side length is 1/10 to 1/20 of the wavelength so that the waveform can be expressed with low error when a space is divided. Therefore, in many cases, it becomes a large-scale problem. In this study, due to the need for electromagnetic compatibility (EMC) evaluation of the surrounding electromagnetic field generated when a microwave scalpel is used in surgery, a large-scale electromagnetic analysis method for the microwave region inside the operating room has been developed. In this paper, the introduced parallel mesh subdivision function enables high-speed mesh generation with hundreds of millions of elements. In addition, this method provided a successful analysis.



## 1. Introduction

In recent years, as the performance of computers and parallel computing technology has improved, electromagnetic field simulation has also seen further evolution, including analysis functions for large spaces. Along with this evolution, demand for the use of electromagnetic field analysis is increasing, not only in conventional industrial applications but also in medical settings, with the aim of improving the safety of medical devices such as microwave scalpels. Among electromagnetic field analyses for high-frequency regions, the mainstream method is a formulation that solves a vector wave equation with the electric field E as an unknown function. To express the electric field waveform, which is the solution obtained by analysis, with low error, it is necessary to divide the process into elements whose maximum side length is 1/10 to 1/20 of the wavelength, which greatly increases the computational scale. Therefore, the authors' research group is researching and developing a full-wave electromagnetic field analysis method based on a parallel finite element method with the domain decomposition method, which is known to be effective for large-scale analysis. Parallelization is essential for large-scale analysis, and this study applies one method, the iterative domain decomposition method.

In this method, the analysis domain is divided into small domains called subdomains, and while finite element analysis is performed for each subdomain, an interface problem is solved to satisfy the equilibrium problem between domains. For subdomain problems, highly efficient parallel computation is possible because the subdomain problems can be calculated independently by applying Gaussian elimination, which is a direct method, and an iterative method between subdomain boundaries. As a method for implementing the iterative domain decomposition method (IDDM) on a parallel computer. The effectiveness of this method in large-scale analysis of high-frequency electromagnetic field problems has been reported in past studies [1-2].

The microwave scalpel, one of the energy devices used in surgery, are useful because they can cut blood vessels without bleeding by irradiating 2.45GHz electromagnetic waves and ensure a clear surgical field. On the other hand, it is known that electromagnetic

*Corresponding author E-mail: takei@cc.miyazaki-u.ac.jp*

interference occurs with other electronic and medical devices present in the operating room. Therefore, a full-scale analysis of the entire operating room is necessary to understand electromagnetic phenomena.

In this study, first, a resonator model was used to determine the appropriate convergence in the gigahertz regions for the matrix iterative solution of the analysis code. Next, by adding the necessary functions for large-scale analysis, such as mesh subdivision using a domain decomposition type data structure, we built a large-scale full-wave electromagnetic field analysis framework that can be applied to the EMC study of large medical electromagnetic environments.

## 2. Formulation of microwave analysis

### 2.1 Vector wave equation

In this study, we considered a vector wave equation in which the electric field $\boldsymbol{E}$ [V/m] derived from Maxwell's equation, which does not ignore displacement current, is unknown, and this equation is used as the basic equation [3-5].

$$rot\{(1/\mu)rot\boldsymbol{E}\} - \omega^2\varepsilon\boldsymbol{E} = j\omega\boldsymbol{J} \qquad in\ \Omega \tag{1a}$$

$$\boldsymbol{E}\times\boldsymbol{n} = \boldsymbol{0} \qquad on\ \partial\Omega \tag{1b}$$

Here, $\omega$ [rad/s] is the angular frequency, $\mu$ [H/m] is the magnetic permeability, $\varepsilon$ [F/m] is the complex permittivity, $\sigma$ [S/m] is the conductivity, $\boldsymbol{J}$ [A/m$^2$] is the current density, $j$ is an imaginary unit, and $\boldsymbol{n}$ is the normal vector. The complex permittivity is given by $\varepsilon = \varepsilon_0\varepsilon_r - \sigma/j\omega$, where $\varepsilon_0$ is the vacuum permittivity and $\varepsilon_r$ is the relative permittivity. These equations are solved by the parallel finite element method. The formulation of the parallel finite element method is discussed in the next section.

### 2.2 Finite element equation

We derive a weak form using the Galerkin method for equation (1) and consider finite element decomposition Ω in the analysis domain. The electric field **E** is approximated by a Nédélec tetrahedral linear element, which is an edge element, and the current density $\boldsymbol{J}$ is approximated by a tetrahedral linear element [6-7]. Let $\boldsymbol{E_h}$ and $\boldsymbol{J_h}$ be the finite element approximations of the electric field $\boldsymbol{E}$ and current density $\boldsymbol{J}$, respectively. $\boldsymbol{E}_h{}^*$ represents any test function.

$$\iiint_\Omega (1/\mu)rot\boldsymbol{E}_h\cdot rot\boldsymbol{E}_h{}^* dv - \omega^2\iiint_\Omega \varepsilon\boldsymbol{E}_h\cdot\boldsymbol{E}_h{}^* dv = j\omega\iiint_\Omega \boldsymbol{J}_h\cdot\boldsymbol{E}_h{}^* dv \tag{2}$$

### 2.3 Domain decomposition method

In this study, we applied the domain decomposition method (DDM) as a parallel computing method for large-scale analysis [8-9]. This method divides the whole domain into several subdomains and divides them into finite element calculations for the internal degrees of freedom of the subdomains and iterative calculations for interface problems that balance the degrees of freedom on the internal boundaries, thereby achieving memory dispersion. This is a very efficient parallelization method that reduces the degrees of freedom solved by an iterative method. We obtain the linear equation (3) to be solved from the finite element equation (2).

$$Ku = f \tag{3}$$

Here, $K$ is a coefficient matrix and a complex symmetric matrix, $u$ is an unknown vector, and $f$ is a known vector. The analysis domain Ω is divided into $N$ parts with no overlap between the domains.

$$\Omega = \bigcup_{i=1}^{N}\Omega^{(i)} \tag{4}$$

The superscript ($i$) is the subdomain number. Hereafter, ($i$) represents data related to $\Omega^{(i)}$. If the determinant is divided into the degree of freedom $u_I^{(i)}$ inside the subdomain and the degree of freedom $u_B$ on the internal boundary and rearranged, the form becomes equation (5).

$$\begin{bmatrix} K_{II}^{(1)} & \cdots & 0 & K_{IB}^{(1)}R_B^{(1)} \\ \vdots & \ddots & \vdots & \vdots \\ 0 & \cdots & K_{II}^{(N)} & K_{IB}^{(N)}R_B^{(N)} \\ R_B^{(1)}K_{IB}^{(N)T} & \cdots & R_B^{(N)}K_{IB}^{(N)T} & \sum_{i=1}^{N} R_B^{(i)}K_{BB}^{(i)}R_B^{(i)T} \end{bmatrix} \begin{bmatrix} u_I^{(1)} \\ \vdots \\ u_I^{(N)} \\ u_B \end{bmatrix} = \begin{bmatrix} f_I^{(1)} \\ \vdots \\ f_I^{(N)} \\ f_B \end{bmatrix} \tag{5}$$

Here, $R_B^{(i)T}$ in equation (5) restricts $u_B$ to $u_B^{(i)}$, which is the internal degree of freedom of the subdomain $\Omega^{(i)}$ 0-1, and it is a matrix. From this, equations (6) and (7) are derived.

$$K_{II}^{(i)}u_I^{(i)} = f_I^{(i)} - K_{IB}^{(i)}u_B^{(i)} \qquad i = 1,\cdots,N \tag{6}$$

$$\left\{\sum_{i=1}^{N} R_B^{(i)}\left\{K_{BB}^{(i)} - K_{IB}^{(i)T}\left(K_{II}^{(i)}\right)^{-1}K_{IB}^{(i)}\right\}R_B^{(i)T}\right\}u_B = \sum_{i=1}^{N} R_B^{(i)}\left\{f_B^{(i)} - K_{IB}^{(i)T}\left(K_{II}^{(i)}\right)^{-1}f_I^{(i)}\right\} \tag{7}$$

Here, $f_B^{(i)}$ is the right-hand side vector regarding $u_B$ and $\left(K_{II}^{(i)}\right)^{-1}$ is the inverse matrix of $K_{II}^{(i)}$.

In addition, equation (7) is called the interface problem, and is an equation for satisfying continuity between domains in the domain segmentation method. For simplicity, equation (7) is rewritten as equation (8).

$$Su_B = g \tag{8}$$

However,

$$S = \sum_{i=1}^{N} R_B^{(i)} S^{(i)} R_B^{(i)T} \tag{9}$$

$$S^{(i)} = K_{BB}^{(i)} - K_{IB}^{(i)T} \left(K_{II}^{(i)}\right)^{-1} K_{IB}^{(i)} \tag{10}$$

Here, $S$ is the Schur complement matrix, $S^{(i)}$ is the local Schur complement matrix in the subdomain $\Omega^{(i)}$, and $g$ is the right-hand vector of equation (7).

### 2.4 Iterative solution method

In this study, an IDDM was applied as a parallelization method [10-11]. The IDDM is a method for solving the interface problem shown in equation (8) using an iterative method such as the conjugate orthogonal conjugate gradient (COCG) method. The COCG method is a well-known iterative algorithm used to solve linear equations very efficiently.

To apply an algorithm based on the COCG method to equation (8), first we calculate the degree of freedom $u_B$ on the internal boundary. δ is the convergence with positive value. In addition, $\|\cdot\|$ represents the 2-norm. Fig. 1 shows the COCG algorithm for the interface problem. In Fig. 1(a) during the initial residual calculation and in Fig. 1(b) for the COCG step, it is necessary to perform a vector product operation of the Schur complement matrix $S$, but compared to the coefficient matrix $K$, constructing the matrix $S$ requires a huge amount of calculation. Therefore, by replacing (a) and (b) with the finite element calculation of the subdomain shown in the lower part of Fig. 1, the matrix $S$ can be calculated without explicitly creating it. Then, by calculating $u_I^{(i)}$ for each subdomain using equation (6), a solution for the entire analysis domain is obtained. Equations (6) and (a) and (b) at the bottom of Fig. 1 can be calculated independently in each subdomain, making parallel calculation possible. Calculations for (a) and (b) are performed using the Gaussian elimination method based with $LDL^T$ decomposition.

Choose $u_B^0$ ;

$$p^0 = r^0 = Su_B^0 - g \; ; \quad \cdots\cdots (a)$$

for $= 0,1,\cdots$ ;

$$q^n = Sp^n \; ; \quad \cdots\cdots (b)$$

$$\alpha^n = \frac{(r^n)^T r^n}{(p^n)^T q^n} \; ;$$

$$u_B^{n+1} = u_B^n - \alpha^n p^n \; ;$$

$$r^{n+1} = r^n - \alpha^n q^n \; ;$$

if $\|r^{n+1}\| < \delta \|r^0\|$ , break;

$$\beta^n = \frac{(r^{n+1})^T r^{n+1}}{(r^n)^T r^n} \; ;$$

$$p^{n+1} = r^{n+1} + \beta^n p^n \; ;$$

end;

In each subdomain (Replacement of eq. $(a)$)

Compute $u_I^{(i)0}$ by

$$K_{II}^{(i)} u_I^{(i)0} = f_I^{(i)} - K_{IB}^{(i)} R_B^{(i)T} u_B^0 \; ;$$

$$r^{(i)0} = K_{IB}^{(i)T} u_I^{(i)0} + K_{BB}^{(i)} R_B^{(i)T} u_B^0 - f_B^{(i)} \; ;$$

$$p^0 = r^0 = \sum_{i=1}^{N} R_B^{(i)} r^{(i)0} \; ;$$

In each subdomain (Replacement of eq. $(b)$)

Compute $p_I^{(i)n}$ by

$$K_{II}^{(i)} p_I^{(i)n} = -K_{IB}^{(i)} R_B^{(i)T} p^n ;$$

$$q^{(i)n} = K_{IB}^{(i)T} p_I^{(i)n} + K_{BB}^{(i)} R_B^{(i)T} p^n \; ;$$

$$q^n = \sum_{i=1}^{N} R_B^{(i)} q^{(i)n} \; ;$$

Fig. 1 IDDM algorithm based on COCG method

## 3. Numerical experiments

### 3.1 Determination of analysis conditions in high-frequency region

The microwave scalpel analyzed with our method uses the thermal effect of a high-frequency electromagnetic field at 2.45GHz, which is the resonance frequency of water, to coagulate proteins in the incision, allowing surgery to be performed without bleeding. This surgical device can reduce the physical burden on the patient.

The error in the electric and magnetic fields calculated by the parallel analysis code used in this study is less than 5%, which is sufficiently accurate [2]. However, there is a concern that the COCG method may cause false convergence depending on the convergence criteria at a specific frequency. There is a large difference between the residual found from the recurrence formula and the true residual found from the approximate solution. If this difference becomes large, even if the residual norm of the recurrence formula continues to decrease, the true residual norm will remain at a constant value, and the accuracy of the approximate solution will not improve. This situation is called false convergence [12]. Therefore, to confirm that calculations can be performed appropriately for the target 2.45GHz electromagnetic field, a frequency response analysis was performed to determine

appropriate convergence criteria in the several-gigahertz region. A schematic diagram and dimensions of the numerical model used for the frequency response analysis are shown in Fig. 2, and model specifications are given in Table 1. To create a resonator, all boundary conditions were set to correspond to completely conductive walls. Also, as given in the literature [11], the number of elements included in each subdomain was set to 300. The computing environment used in this analysis was a PC cluster equipped with an Intel Core i7 multi-core CPU and 32GB of memory, and 20 computer nodes (80 cores) were used.

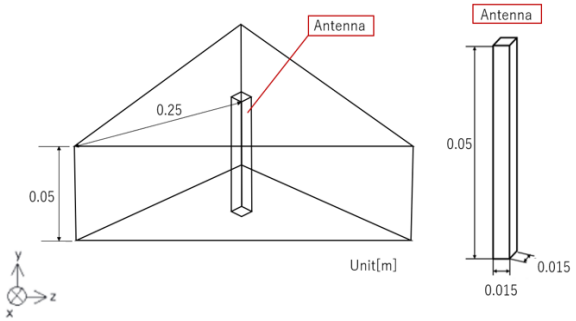


Fig. 2 Resonator model

Table 1 Specifications of resonator model

| Number of elements | Number of nodes | Number of subdomains |
|---|---|---|
| 1,590,759 | 2,219,723 | 300×67 |

First, a frequency response analysis was performed using the convergence criterion $\delta = 1.0 \times 10^{-3}$. The analysis range was 2GHz to 3GHz, and execution was performed in 10MHz increments. Fig. 3 shows the results of the frequency response analysis of the electric field.

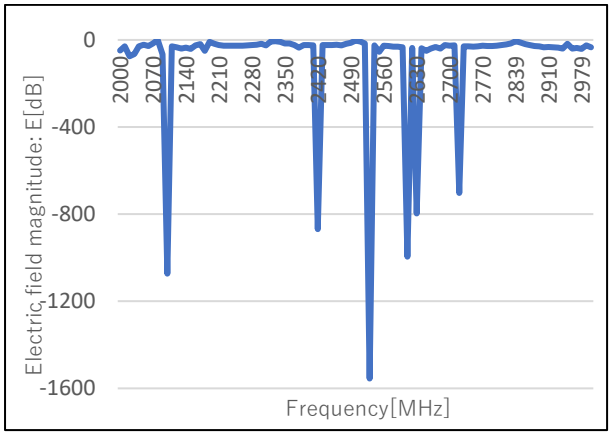


Fig. 3 Results of frequency response analysis in gigahertz region

From Fig. 3, false convergence occurs at a total of six frequencies. Fig. 4 shows a plot of the graph in Fig. 3 excluding the frequencies that caused false convergence.

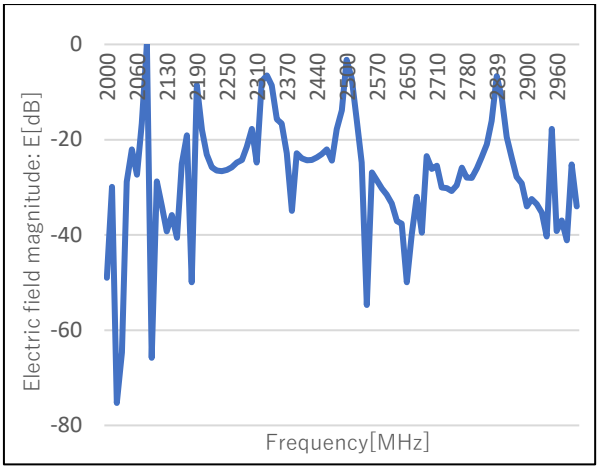


Fig. 4 Results of frequency response analysis after false convergences are excluded

Fig. 5 shows the visualization results of the frequencies of the top two resonance points, 2080MHz and 2500MHz, which can be seen from Fig.4. In addition, at frequencies where false convergence occurred, the analysis was performed with the convergence criterion $\delta = 1.0 \times 10^{-5}$. Fig. 6 shows a comparison of the visualization results at 2100MHz and 2530MHz.

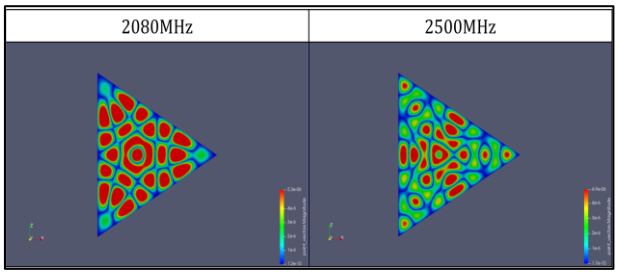


Fig. 5 Visualization result at the resonance point

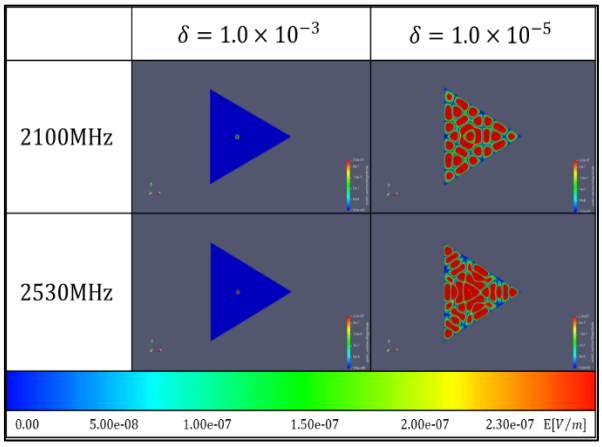


Fig. 6 Visualization comparison at false convergence frequencies

The data presented above confirm that appropriate results are obtained with the convergence criterion $\delta = 1.0 \times 10^{-3}$, but at a certain frequency false convergence occurs and the convergence criterion $\delta = 1.0 \times 10^{-5}$ provides appropriate results. Therefore, in the simulation of a real environment, if false convergence is

found after checking the calculation results, recalculation can be performed with a smaller convergence criterion.

### 3.2 Analysis assuming a real environment

In this study, a situation was set up assuming the use of a microwave scalpel in the obstetrics and gynecology operating room of our university's medical school. The size of the operating room was assumed to be 6.3 meters wide, 6.7 meters deep, and 3.0 meters high, and there is an antenna in the center of the room and a column imitating a human body that is assumed to be a patient, doctor, and nurse. Fig. 7 shows a schematic diagram of the actual operating room. When the analysis frequency is set to 2.45GHz, which is the female specification, it is estimated that approximately 2.8 billion elements will be required if elements are divided with the maximum side length being 1/20 of the wavelength for waveform approximation. Therefore, for parallelization, we created a model with fewer elements by dividing the domain while performing mesh subdivision [13-14]. Fig. 8 shows the flowchart of the mesh subdivision.

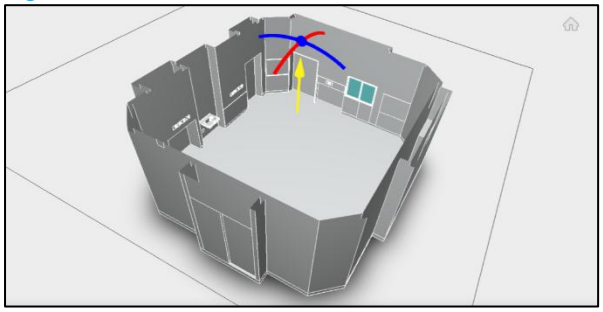

Fig. 7 Operating room model

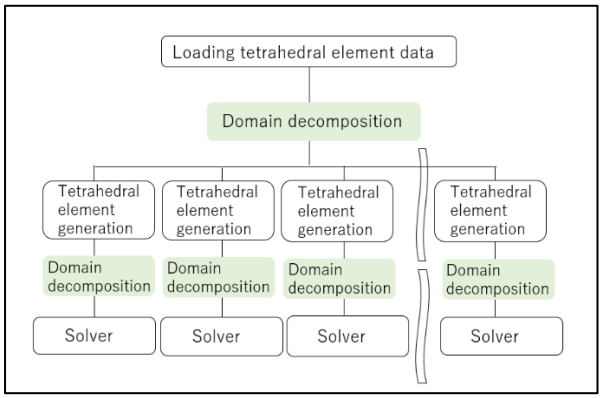


Fig. 8 Mesh subdivision flowchart

This time, the model was created by mesh subdivision three times. The number of elements after each subdivision is shown in Table 2. Table 3 shows the model specifications and analysis conditions. To create an operating room model, all boundary conditions were set to correspond to completely conductive walls.

Table 2 Number of elements in model created by subdivision

| | Elements |
|---|---|
| Before subdivision | 5,724,522 |
| After subdivision once | 45,796,176 |
| After subdivision twice | 366,369,40 |
| After subdivision thrice | 2,930,955,264 |

Table 3 Model specifications and analysis conditions

| Elements | Analysis frequency | Convergence criterion |
|---|---|---|
| 5,724,522 | 300MHz | $1.0 \times 10^{-3}$ |

Table 4 shows the time required to create model models. The model of approximately 366 million elements was approximately 66 minutes (= approximately 36 minutes for mesh generation of tetrahedral elements + approximately 30 minutes for one subdivision). In contrast, a model with approximately 100 million elements could be created without using the subdivision function, but the processing was not completed even after more than 4 days. From this result, creating a model with about 366 million elements will take even more time. On the other hand, by incorporating the mesh refinement function, the time required to create the model can be significantly reduced.

Table 4 Time required to create numerical models

| | 366 million elements model | 100 million elements model |
|---|---|---|
| Mesh generation | 36 min | 4 days or more |
| Subdivision | 30 min | |
| Total time | 66 min | Unable to create model |

In this study, we first performed the analysis using the model before subdivision. The analysis frequency is assumed to be a device between a microwave scalpel. As described above, $\delta = 1.0 \times 10^{-3}$ generally provides valid convergence. However, when the obtained calculation result caused false convergence, the convergence criterion was decreased to $\delta = 1.0 \times 10^{-5}$ and the calculation was repeated. In addition, the number of elements included in each subdomain was set to 300 [11]. The computer environment used in this analysis was a PC cluster equipped with an Intel Core i7 multi-core CPU and 32GB of memory, and 19 computers (76 cores) were used. Fig. 9 shows the visualization results for the electric field, and Table 5 shows the calculation results.

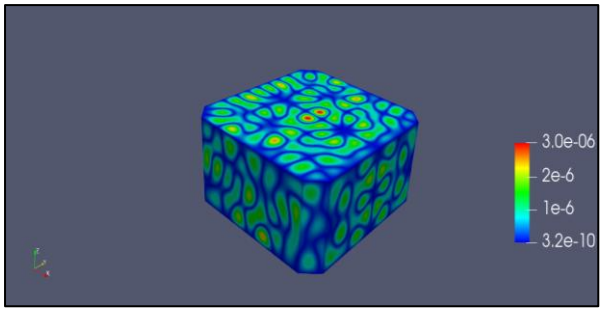


Fig. 9 Visualization results for electric field in operating room model

Table 5 Operating room model calculation results

| Elapsed time [s] | Number of iterations | Amount of memory used [GB] |
|---|---|---|
| 7,880 | 61,270 | 6.3 |

As can be seen from Table 5, the elapsed time was nearly 2days, and the number of iterations was 61,270. Next, analyzed the one-subdivision model. Table 6 shows the model specification and analysis conditions. Analysis of this model is currently being performed on a PC cluster equipped with an Intel Core i7-9700K multi-core CPU (3.60GHz) and 36 GB of memory, and 20 computers (160 cores). Table 7 shows the calculation results for the one-subdivision model. In addition, Fig. 10 shows its convergence history of the relative residual norm.

Table 6 Model specifications and analysis condition for one-subdivision model

| Elements | Analysis frequency | Convergence criterion |
|---|---|---|
| 45,796,176 | 300MHz | $1.0 \times 10^{-3}$ |

Table 7 Operating room model calculation results for one-subdivision model

| Elapsed time [s] | Number of iterations | Amount of memory used [GB] |
|---|---|---|
| 125,046 | 330,210 | 53.6 |

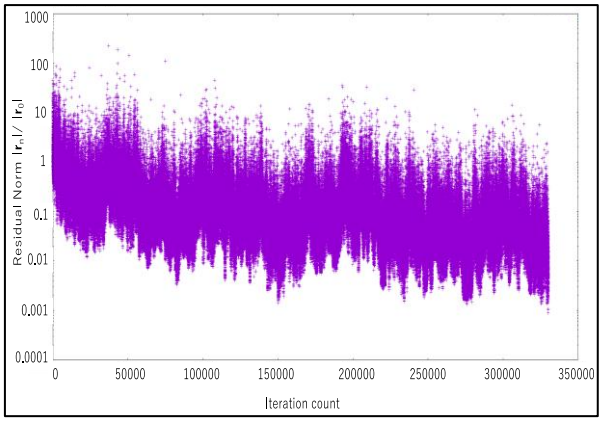


Fig. 10 Convergence history for one-subdivision model

The model after subdivision had approximately 366 million elements, which is eight times the number of elements in the original model and is expected to take even more calculation time.

In the future, we plan to further reduce the number of calculations from the current analysis code by improving the algorithm, such as introducing quadratic edge elements and a sparse matrix direct method as a subdomain solving method.

## 4. Summary

This paper describes the basic equations, calculation algorithms, and calculation accuracy of the analysis code used for high-frequency electromagnetic field analysis. We investigated appropriate convergence through frequency response analyses in the several gigahertz regions, including 2.45GHz, which is the specification for microwave scalpels.

Furthermore, after selecting appropriate analysis conditions from the initial study, we created a model using the mesh subdivision function, performed analysis on the model before subdivision, and confirmed that the calculations were performed appropriately. After this, analysis using the large-scale model after mesh refinement was performed. As future work, we plan to reduce the amount of calculation by improving the calculation algorithm, such as introducing higher-order elements and changing the subdomain solution method.

## Acknowledgment

Part of this research was supported by the Japan Science and Technology Agency's Research Results Optimal Deployment Support Program [A-STEP (Tryout), JPMJTM22ER]. In addition, part of this research is related to joint research with Sony GM&O Corporation, titled "Research on high-speed solution methods for ultra-large-scale high-frequency electromagnetic field analysis."

## References


1. A. Takei, S. Yoshimura, H, Kanayama: "Large-Scale Parallel Finite Element Analyses of High Frequency Electromagnetic Field in Commuter Trains," *CMES*, vol.31, no.1, pp.13-24, 2008.
2. A. Takei, M. Ogino, S. Sugimoto: "High-frequency electromagnetic field analysis by COCR method using anatomical human body models," *IEEE Trans. on Mags*, vol.54, no.3, 2018.
3. P. Liu, and Y. Q. Jin: "The Finite-element Method with Domain Decomposition for Electromagnetic Bistatic Scattering from the Comprehensive Model of a Ship on and a Target Above a Large-scale Rough Sea Surface," *IEEE Trans. Geos*., vol.42, no.5, pp.950-956,
4. Y. J. Li, and J. M. Jin: "Implementation of the Second-Order ABC in the FETI-DPEM Method for 3D EM Problems," *IEEE Trans. Antennas and Propag.*, vol.56, no.8 pp. 2765-2769, 2008.
5. T. Ha, S. Seo, D. Sheen: "Parallel Iterative Procedures for a Computational Electromagnetic Modeling Based on a Nonconforming Mixed Finite Element Method," *CMES*, vol. 14, no. 1, pp. 57-76, 2009.
6. F. Kikuchi: "Numerical Analysis of Electrostatic and Magnetostatic Problems," *Sugaku Expositions*, vol.6, no.1, pp.33-51, 1993.
7. H. Kanayama, S. Sugimoto: "Effectiveness of A-$\phi$ Method in a Parallel Computing with an Iterative Domain Decomposition Method," *IEEE Trans. Mags.*, vol. 42, no. 4, pp. 539-542, 2006.
8. A. Takei, K. Murotani, S. Sugimoto, M. Ogino, T. Yamada, S. Yoshimura: "Performance evaluation of parallel finite element electromagnetic field analysis using numerical human models," Journal of Advanced Simulation in Science and Engineering, vol.1, no.1,
9. J. Mandel: "Balancing domain decomposition, Communications on Numerical Methods in Engineering," vol.9, pp.233-241, 1993.
10. A. Takei, K. Murotani, S. Sugimoto, M. Ogino and H. Kawai: "High-accuracy electromagnetic field simulation using numerical human body models," *IEEE Trans. on Magns*, vol.52, no.3, DOI: 10.1109/TMAG.2015.2479467, 2016.
11. K. Ohnaka, N. Mizoguchi, T. Murayama, S. Goto and A. Takei: "Large-Scale High-Frequency Electro magnetic Simulation Based on Domain Decomposition Type Parallel Finite Element Method," *JSST*, vol.15, no.2, pp. 87–93, 2023. (in Japanese)
12. K. Aihara: "Reducing the residual gap in short recurrence," *RIMS Kokyuroku*, vol. 2094, pp. 112-121, 2018. (in Japanese)
13. K. Murotani, S. Sugimoto, H. Kawai and S. Yoshimura: "Hierarchical Domain Decomposition with Parallel Mesh Refinement for Billons-of-DOF Scale Finite Element Analysis," International Journal of Computational Methods, vol.11, no.04, 2014
14. G. Gibert, B. Prabel, A. Gravouil, Clémentine Jacquemoud: "A 3D automatic mesh refinement X-FEM approach for fatigue crack propagation," Finite Elements in Analysis and Design, vol.157, pp.21-37, 2019.


## Authors Introduction


Ms. Nanako Mizoguchi

She received her B.S. degree in Engineering in 2023 from the Faculty of Engineering, University of Miyazaki in Japan. She is a master course student of Graduate school of Engnnering, University of Miyazaki in Japan. Her main research is on large-scale high frequency electromagnetic field analysis methods based on the parallel finite element method.

Mr. Kento Ohnaka

He received his B.S. degree in Engineering in 2022 from the Faculty of Engineering, University of Miyazaki in Japan. He is a master course student of Graduate school of Engnnering, University of Miyazaki in Japan. His main research is on large-scale high frequency electromagnetic field analysis methods based on the parallel finite element method.

Mr. Hironobu Sugiyama

He is a distinguished Assistant Professor in the Department of Medical Environmental Innovation at the University of Miyazaki and a senior manager in the Medical Division at NIKKISO Co., LTD. He is conducting research and development of medical devices. He holds master's degree in engineering from Hokkaido university and his specialty is bioengineering.

Prof. Shouichi Fujimoto

He graduated from Yamaguchi University School of Medicine in 1979 and received his medical license (M.D.). Then, he received his Ph.D. in 1990 from the Faculty of Medicine, University of Miyazaki. He is currently a Distinguished Professor in the Department of Medical Environmental Innovation at the University of Miyazaki. He specializes in Nephrology and Dialysis Medicine and practices as a board-certified physician.

Mr. Sota Goto

He received his B.E. degree from Keio University in 2020, M.S. degree from the University of Tokyo in 2022. He joined Sony Corporation in 2022, and has been engaged in research and development of electromagnetc field simulators at Sony Global Manufacturing & Operations Corporation since then. His research interests include large-scale electromagnetic field analysis methods and Uncertainty Quantification (UQ).

Dr. Toshio Murayama

He received his B.E. degree from the University of Tokyo in 1987,M.S. degree from the University of California at Santa Barbara in 1991 and Ph. D. degree in engineering from the University of Tokyo in 2012. He joined Sony Corporation in 1987. He has been researching numerical analysis of electromagnetics. His research interest covers also multi-domain circuit electromagnetic co-simulation.

Prof. Amane Takei

He is working as Professor for Department of Electrical and systems Engineering, University of Miyazaki, Japan. His research interest includes high performance computing for computational electromagnetism, iterative methods for the solution of sparse linear systems, domain decomposition methods for large-scale problems. Prof. Takei is a member of IEEE and JSST, an expert advisor of IEICE, a delegate of IEEJ.